RESEARCH ARTICLE

Correspondence to:
D. Seidov,
dan.seidov@noaa.gov

Eddy-Resolving In Situ Ocean Climatologies of Temperature and Salinity in the Northwest Atlantic Ocean

Dan Seidov[1] (iD)**, Alexey Mishonov[1,2]** (iD)**, James Reagan[1,2]** (iD)**, and Rost Parsons[3]** (iD)

[1]National Centers for Environmental Information, NOAA, Silver Spring, MD, USA, [2]Earth System Science Interdisciplinary Center/Cooperative Institute for Climate and Satellites-Maryland, University of Maryland, College Park, MD, USA, [3]Stennis Space Center, National Centers for Environmental Information, NOAA, Hancock County, MS, USA

Abstract Circulation patterns and thermohaline fields of the Northwest Atlantic are highly variable in space and time and are strongly impacted by various mesoscale phenomena such as quasi-stationary frontal zones with sharp gradients, meandering jet-like currents, vortexes, and filaments. These all contribute to building and maintaining complex large-scale regional structures of ocean tracers, such as temperature and salinity, which persist over time periods of decades and longer. To reflect the existence of these long-term mesoscale phenomena and diagnose their changes, a new high-resolution in situ climatology of the Northwest Atlantic was developed. At its core, this eddy-resolving climatology, with 1/10° horizontal resolution, reveals a cumulative effect of mesoscale dynamics within the Northwest Atlantic. Additionally, strong agreement exists between this in situ climatology and climatologies derived from high-resolution satellite data, thus providing a validation of the presence of stochastic periodicity of ocean tracer patterns on decadal timescales. Furthermore, large and very localized multidecadal subsurface heat gains southeast of the Gulf Stream was diagnosed using this new high-resolution regional climatology. It was demonstrated that the climatic shifts in the wind stress over the Northwest Atlantic may play a leading role in this heat accumulation due to subtropical water heaving through Ekman pumping. It is argued that uncovering many important details of long-term ocean climate variability from in situ ocean data can only be ascertained through the use of eddy-resolving climatologies.

Plain Language Summary Historically, the long-term state of the global ocean, particularly for temperature and salinity, has been derived from in situ observational data and mapped to rather coarse horizontal resolutions of 1° and more recently to 1/4°. Most mesoscale activity, such as the meandering of jet streams, eddies, large vortexes, and filaments, cannot be adequately mapped with such resolutions. Unfortunately, in most places in the World Ocean a better resolution is unattainable due to limited observations. However, in a small number of ocean regions higher-resolution mapping is now possible. These regions are well sampled and in many cases are extremely important for the ocean and Earth's climate. The Northwest Atlantic is one of these regions. Using a large volume of temperature and salinity data, a new decadally averaged high-resolution (with 1/10°) ocean climatology was compiled for this region and used, in conjunction with ancillary data, to assess ocean climate change and decadal variability in this region with higher accuracy over the past six decades.

1. Introduction

Monthly, seasonal, and annual values of seawater parameters, for example, temperature and salinity, mapped onto regular spatial grids at specified depth levels and averaged over sufficiently long periods of time (decades and longer) are called "ocean climatologies"—a term first used in Levitus (1982) to describe the long-term mean state of the ocean. The regional ocean climatologies discussed in this study are a subset of the World Ocean Atlas (WOA), a global ocean climatology of many parameters. A brief review of WOA's evolvement from the first edition in 1982 under the name of *Climatological Atlas of World Ocean* (Levitus, 1982) to WOA13 v2 published in 2013 (https://www.nodc.noaa.gov/OC5/woa13/) can be found in Seidov et al. (2018). All WOA editions are compiled using ocean profiles data archived in the *World Ocean Database* which is published and maintained by NOAA's National Centers for Environmental Information (NCEI; https://www.nodc.noaa.gov/OC5/WOD/pr_wod.html).

All WOA editions were compiled using a procedure widely known in geophysics as objective analysis of irregularly distributed data (Barnes, 1973; Boyer et al., 2005; Thomson & Emery, 2014). The goal of this procedure

Table 1

Radii of Influence Used in NWA Climatologies' Objective Analysis for 1° × 1°, 1/4° × 1/4°, and 1/10° × 1/10° Grids (Updated From Boyer et al., 2005; See Also Seidov et al., 2016, 2018)

Pass	Radius of influence (km)		
	1° × 1° grid	1/4° × 1/4° grid	1/10° × 1/10° grid
1	892	321	253
2	669	267	198
3	446	214	154

Note. NWA = Northwest Atlantic.

is to use data that are nonuniform in time and space to create relatively smooth yet realistic fields of ocean variables on a regular grid. It ensures that all grid cells without observed data (i.e., "data gaps") are filled using weighted differences between the statistical mean and a first-guess field. The entire procedure can be seen as "mapping" of the ocean's essential parameters (temperature, salinity, oxygen, nutrients, etc.) on a regular grid using all available data (see Seidov et al., 2018). Two significant elements of the objective analysis are the first-guess field and radius of influence. The choice of the first-guess field is of paramount importance, especially where data density is low. The radius of influence is equally if not more important. The more data available within the radius of influence, the more weight the observed data gain relative to the first-guess values (see Table 1 and, e.g., Boyer et al., 2005; Locarnini et al., 2013; Seidov et al., 2016, 2018).

This approach works best with no or relatively few gaps in data coverage, and if the gaps do exist, there are enough data in neighboring cells to fill empty cells confidently (Boyer et al., 2005; Levitus, 1982). Data coverage on a 1° resolution grid in data-rich regions would have very few, if any, data gaps on the decadal timescale. While climatological fields at 1° resolution are still adequate for many scientific applications, present-day ocean models and many regional research projects demand significantly finer-resolution data mapping. Unfortunately, only a few areas in the World Ocean exist where the observation density is sufficient to allow finer than 1° spatial resolutions data mapping. Although this may limit the spatial range of high-resolution mapping, the mandates for better data coverage often coincide with regions that are researched most. Among such, for example, are the East and West Coasts of the United States and Canada, Gulf of Mexico, Gulf of Maine, Bays of Nova Scotia, Greenland-Iceland-Norwegian Seas, and some other locations.

Moving toward fulfilling the requirements for a higher-resolution ocean mapping, a new edition of WOA, named WOA13, was published in 2013 with two spatial grid resolutions—1° × 1° and 1/4° × 1/4° at 102 depth levels, instead of 1° × 1° at 33 levels in all previous editions (Boyer et al., 2014; Locarnini et al., 2013; Zweng et al., 2013). In most of the World Ocean, a grid resolution finer than 1° does not provide across the board improvements because of data insufficiency (see data distribution on 1/4° × 1/4° grid in the WOA13 at https://www.nodc.noaa.gov/OC5/woa13/). On the contrary, in regions with a comparatively high density of observations, a substantial improvement in the 1/4° × 1/4° version of WOA13 compared to the 1° × 1° version was achieved (Boyer et al., 2014). In some of those data-rich regions, a greater level of detail can be reached with an even finer resolution of 1/10° × 1/10° (several examples can be found at NCEI's regional climatology homepage: http://www.nodc.noaa.gov/OC5/regional_climate/). Of all such regions, the Northwest Atlantic (NWA) has perhaps the densest data coverage and was therefore selected as a testing field for employing a new NWA regional climatology (NWARC) in a regional multidecadal ocean climate change study on the grids with 1/4° × 1/4° and 1/10° × 1/10° resolutions (see brief description in Seidov et al., 2018). The NWARC maps and data are available at https://www.nodc.noaa.gov/OC5/regional_climate/nwa-climate/.

Mesoscale eddies are often referred to as energetic ocean currents with the size of about 100 km (Rhines, 2001). A parameter called the Rossby baroclinic radius of deformation R (e.g., Gill, 1982) provides the condition for resolving oceanic mesoscale motion in numerical models or in ocean data mapping. The grid size needed for resolving mesoscale motion must be smaller than R. In the middle latitudes, R is ~30–40 km, which is roughly the latitudinal dimensions of one to two grid cells with 1/4° × 1/4° resolution (~25-km spatial resolution in latitude). A hydrographic front ~50–70 km wide, which is approximately the width the Gulf Stream, can be relatively well resolved on a 1/10° × 1/10° grid (~10-km spatial resolution in latitude and ~8 km in longitude in midlatitudes) and would be just barely visible or "permitted" on the 1/4° × 1/4° grid. Such a front would be completely unresolved at coarser resolutions (e.g., 1° × 1° with scale of ~100 km in latitude).

2. The NWA Thermohaline Structure and Ocean Circulation

The NWA ocean circulation is very complex hosting essential elements of the entire North Atlantic (NA) circulation system, including the fundamentally important Atlantic Meridional Overturning Circulation (AMOC; e.g., Buckley & Marshall, 2016). Figure 1 schematically illustrates the major NWA currents, that is,
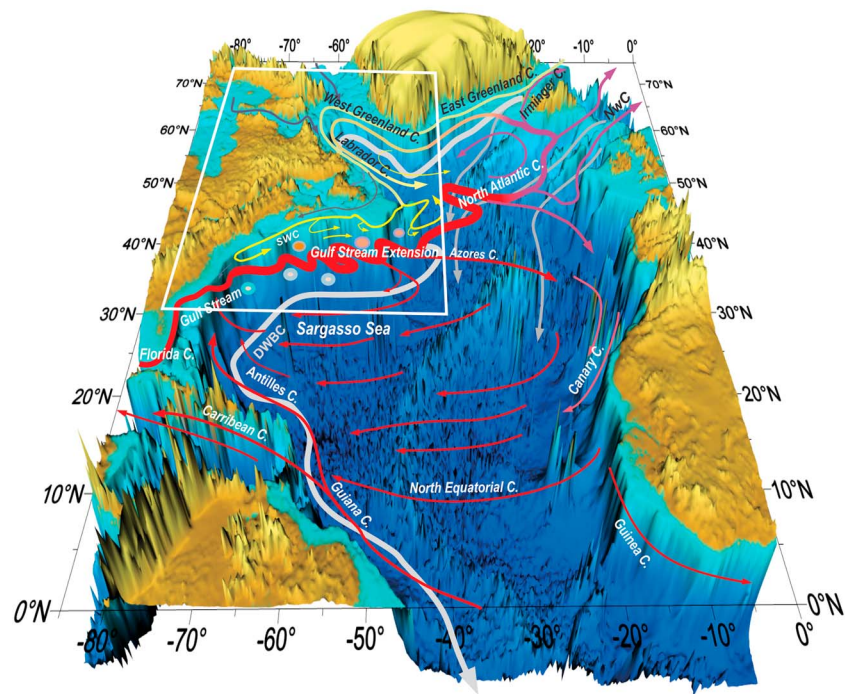
Figure 1. Schematic view of the ocean circulation in the North Atlantic. Warm and cold Gulf Stream rings are shown as small orange and blue circles north and south of the Gulf Stream. Red arrowed vectors indicate major warm surface currents, yellow arrowed vectors indicate major cold surface currents, and gray arrowed vectors show major deep currents. The white box outlines the NWA domain. Abbreviations: NwC = Norwegian Current, IC = Irminger Current, SWC = Slop Water Current, DWBC = Deep Western Boundary Current.

the Gulf Stream System, NA Current, Labrador Current, Slope Water Current, and Deep Western Boundary Current. They are all or partly contained within the NWARC domain shown as a white rectangle in Figure 1.

The Gulf Stream Current System is perhaps one of the most thoroughly explored and charted ocean current systems to date (Richardson, 2001). By the middle twentieth century, oceanographers had already gained rather detailed knowledge of the Gulf Stream, especially in close vicinity to the U.S. East Coast (Fuglister, 1963; Iselin, 1936; Iselin & Fuglister, 1948; Stommel, 1958), with much added insight attained in recent years through a multitude of international observing programs (Yashayaev et al., 2015) and as a part of an intense observing and modeling effort to better understand the AMOC (Buckley & Marshall, 2016).

As the scheme in Figure 1 portrays, the Gulf Stream begins as a confluence of the Florida and Antilles currents. There are cold and warm Gulf Stream recirculation gyres to the north and south of the eastbound Gulf Stream extension (the east part of the Gulf Stream beyond 45°W). Further downstream, the Gulf Stream extension splits into the NA and Azores currents (Hogg & Johns, 1995; Richardson, 2001; Schmitz & McCartney, 1993; Wunsch, 1978). The cold water of the Labrador Sea flows westward along the Newfoundland-Nova Scotia-Northeast U.S. Coasts. This flow is also known as the Slope Water Current. The warm water between 55°W and 75°W, southeast of the Gulf Stream and its extension, recirculates within and around the Sargasso Sea and comprises the Gulf Stream Recirculation Gyre (Hogg et al., 1986; Worthington, 1976).

The position of the Gulf Stream path after separation from U.S. East Coast varies seasonally (Cornillon, 1986; Joyce & Zhang, 2010; Rossby, 1999; Taylor & Stephens, 1998). In the fall, the path migrates to the north, while in the spring it moves to the south relative to its mean annual position. The annual mean path also varies interannually (e.g., Cornillon, 1986; Taylor & Stephens, 1998), although its decadally averaged annual mean position is remarkably stable (Seidov et al., 2017).

East of 75°W, the Gulf Stream is a free baroclinic jet with a great deal of mesoscale activity and increasingly large meanders. By 65°W, the amplitudes of the meanders are nearly 500 km wide, which is almost 10 times

the jet width at the separation point near Cape Hatteras. Although the Gulf Stream and its extension serve as an effective barrier between warm and cold waters along its edges, some blending of those waters is enabled by meanders and mesoscale eddies (Bower et al., 1985). Further mixing occurs through submesoscale streamers enabling the transition from eddy-induced mesoscale geostrophic mixing to smaller-scale turbulent mixing. New studies show that this type of mixing is of particular importance at the Gulf Stream North Wall, where the warm outer core of the Gulf Stream interacts with the cold water originating from the Labrador Sea (e.g., Gula et al., 2016; Klymak et al., 2016).

Through years of dedicated regional observation programs in the NWA (a short review in Yashayaev et al., 2015) and years of eddy-resolving modeling efforts, a consensus was reached that the mesoscale eddies modify the mean circulation in regions of intense baroclinic currents. The mean circulation and mean structure of the ventilated thermocline therefore strongly differs in ocean models when switching from 1° to 1/9° (or even finer) resolution (Lévy et al., 2010). In our analysis, we contend that the structure of the observed ocean climatologies, if compiled with sufficiently fine resolution, should reflect the impact of mesoscale eddies similar to how the long-term averaged ocean tracers are impacted by the mesoscale motion in eddy-resolving ocean models.

3. NWARC

The high-resolution versions of the NWARC, on 1/4° and 1/10° grids, provide a more precise depiction of the ocean climate state and its variability with details not attainable in coarser-resolution analyses. After the first assessment of NWARC capabilities, a hypothesis was put forth that the *seasonal signal carries the superimposed repetitive mesoscale signals and thus decadal climatologies—monthly, seasonal, and annual—reflect the cumulative effect of mesoscale dynamics on mapping of the large-scale regional ocean climate state and variability* (Seidov et al., 2016, 2018, 2017).

The NWARC domain is bounded by 80.0°W and 40.0°W longitudes and 32.0°N and 65.0°N latitudes which enclose the most dynamic and complex current systems of the western NA (white rectangle in Figure 1). The NWARC is a set of analyzed temperature and salinity fields with additional statistical parameters mapping the state of the ocean and aimed at assessing the long-term climatological changes in the NWA area. The NWARC is compiled similarly to the WOA13 as described in Locarnini et al. (2013) and Zweng et al. (2013). It includes six decadal climatologies, from 1955–1964 to 2005–2012. (The climatology of 2005–2012 covers only 8 years because of the WOA13 cutoff time.) The NWARC maps and data are available for viewing and downloading at https://www.nodc.noaa.gov/OC5/regional_climate/nwa-climate/.

Since the NWARC is a subset of WOA13, all elements, structure, and techniques inherent in WOA13 are found in NWARC. The following brief description of the NWARC mostly follows the detailed discussion in the WOA13 publications (e.g., Locarnini et al., 2013; Zweng et al., 2013) and in Seidov et al. (2016). Each monthly decadal climatological parameter (temperature, salinity, etc.) is calculated as an average of each month over 10 years (for the last "decade"—over only 8 years). Averaging every three consecutive decadal months provides four decadal seasons beginning with the winter season defined as January-February-March. The yearly or annual decadal fields are computed as the average of four decadal seasons. The decadal monthly climatologies are defined for the upper 57 of the WOA13 standard depth levels (see https://data.nodc.noaa.gov/woa/WOD13/CODES/PDF/standard_depths.pdf for details) or from the surface to 1,500 m. Seasonal and annual means are computed as averages of monthly fields above 1,500 m with annual means computed as averaged seasonal (without monthly) fields from 1,500 to 4,000 m.

Although data coverage is much denser in the NWA than in most regions of the World Ocean, the availability of temperature and salinity profiles varies in space and time within the NWA domain quite substantially (Seidov et al., 2016). The differences in data coverage over decades are largely due to the evolution in observation systems. The modern equipment, such as Argo profiling floats (Roemmich & Argo-Steering-Team, 2009), covers wider areas (Argo program aims at near-global coverage at 3° × 3° observation resolution), especially away from the coastline but at the expense of fewer focused local observations, which were characteristic of dedicated regional studies of the Gulf Stream in the 1960s to 1970s and of the mesoscale ocean eddies in the 1970s to 1980s (Yashayaev et al., 2015). Data from Argo floats help to close the gaps outside the areas of intense ship-based observations. For example, the Labrador Sea was far better covered in 1995–2004 than in 1965–1974, with improved coverage due to the introduction of

Argo floats (e.g., Roemmich et al., 1998; Steven et al., 2017). At the same time, the Gulf Stream area between Florida Strait and Cape Hatteras was better covered in the 1950s through 1980s, when many special programs studying the Gulf Stream system were operational (e.g., Fofonoff, 1980; Stommel, 1958). There have been several successful attempts to reconstruct key ocean circulation parameters (temperature, salinity, and current velocities) using real and virtual (simulated within a numerical model) Argo floats (e.g., Chapman & Sallée, 2017; Kamenkovich et al., 2011; Koszalka & LaCasce, 2010; LaCasce, 2008). The mean temperature and salinity fields reconstructed from Argo profiling floats were shown to be substantially modified by mesoscale eddies. It corroborates our assertion (see the following sections) that the heat and salt patterns and variability, including long-term heat and salt content change, cannot be properly reconstructed from observations without explicitly resolving mesoscale structures. It should be noted that although this approach in simulating observations shows promise, the entire Argo program covers only the last two decades (with full coverage achieved just ~13 years ago) and thus is insufficient for long-term (several decades) ocean climate change studies. In contrast, the NWARC provides ~60 years of observations. The monthly data coverage maps for each of the six decades showing all observations by all instruments for all three grids in NWARC at all standard depth levels can be viewed at https://www.nodc.noaa.gov/OC5/regional_climate/nwa-climate/.

One of the primary goals of NWARC was to find out if the cumulative effects of mesoscale eddies, meanders, filaments, and rings would become evident in high-resolution mapping on decadal and longer timescales (we consider any climatology on a grid coarser than 1/4° × 1/4° as a "coarse-resolution" climatology). Presumably, the *cumulative effect* of the mesoscale motion emerges in the in situ mapping as long-term averaged repetitive mesoscale elements—meanders, eddies, filament, etc.—that develop quasiperiodically. These elements tend to appear in approximately the same locations, so the averaging over a long period, for example, a decade, would show their stochastic presence even though individual elements cannot be identified in the averaged fields.

In order to identify quasiperiodic mesoscale elements in decadal climatologies, measurements, which capture the hydrographic properties at that particular time, within or in nearby grid cells would need to be made every month throughout the 10 years. However, regardless of how many and/or how frequently the measurements were made, if the values are averaged over space with the resolution of 1° × 1° or coarser, the mesoscale features (shorter than ~100 km in size; e.g., Rhines, 2001) cannot be captured. At 1/4° × 1/4° resolution, the mesoscale elements would be barely seized, whereas on the 1/10° × 1/10° and finer grids they would be reasonably well represented.

The concept of space-time averaging in a statistically steady turbulent flow, when applied to mesoscale motion in the ocean (sometimes referred to as "geostrophic turbulence"; Cushman-Roisin & Tang, 1990; Rhines, 1979), falls within the definition of space-time homogeneity best described by ergodic hypothesis. In its simplest form, it implies that a dynamic system is ergodic if, while being averaged over time, it behaves as if it was averaged over all system's states in its phase space (Monin, 1986; Monin & Yaglom, 1971).

On this point, it is important to understand how the decadal monthly climatologies in WOA and in all NCEI regional climatologies are derived. For a chosen decade, all data with a selected month time stamps for any year in the entire decade are considered to belong to one snapshot of the entire area, in our case the NWA. Effectively, it means that the averaging over any selected area is replaced by averaging over time. For example, all data with a time stamp between 1955 and 1964 for a selected month (i.e., September) would be used to compute the decadal monthly value of the observed parameter (temperature, salinity, etc.), which can be called an "ensemble average." All temperatures with the September time stamp within the decade 1955–1964 would be used for calculating the ensemble average of temperature in each cell of this grid. The simplest method would be to compute a mean of the monthly decadal temperature in this cell by averaging all monthly temperature observations within this cell for the selected decade. Using the objective analysis procedure after monthly averaging over the cell volume (as we use all data with the specified time stamp within a cell) does not change the fundamental principle of replacing the ensemble average, that is, averaging over both time and space, by time average based on the assumption that the ocean climate system is an ergodic system (Monin, 1986). Hence, to "eddify" a climatology, we simply select a grid with a spatial resolution that allows mesoscale disturbances to be explicitly included and not filtered out by the
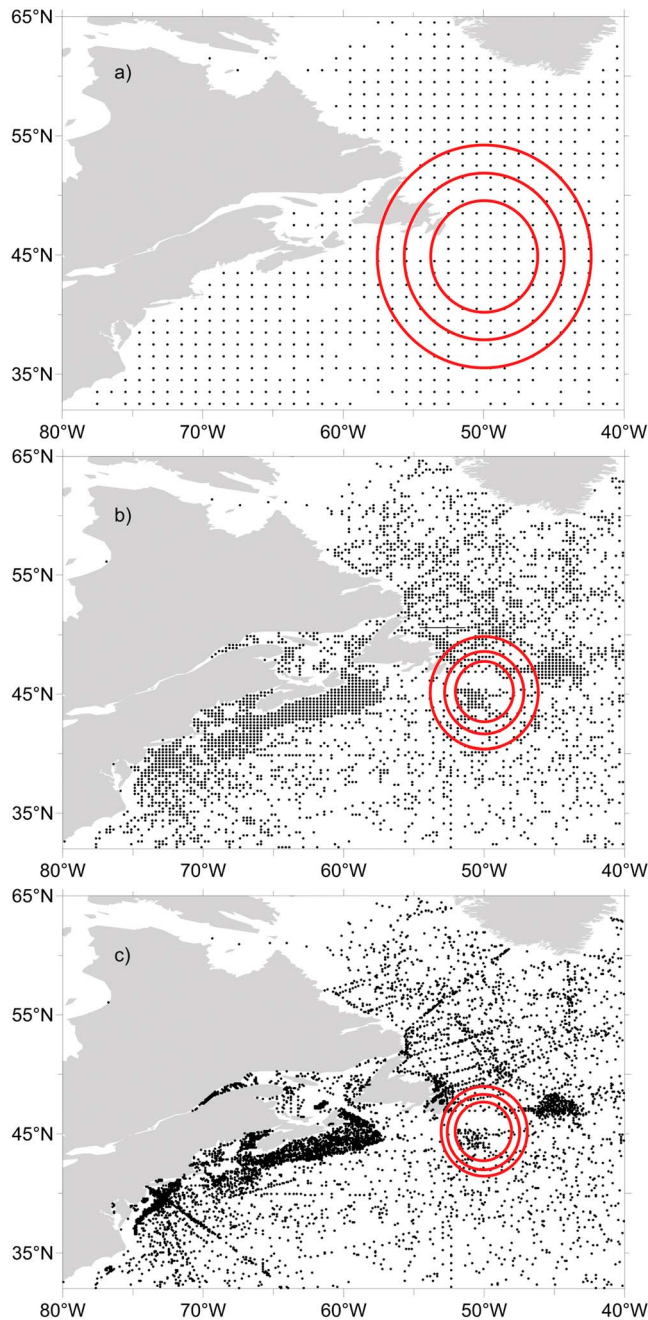
Figure 2. Temperature observation density at 10-m depth for the decadal July of 1995–2004 on grids of: (a) 1° × 1°, (b) 1/4° × 1/4°, and (c) 1/10° × 1/10° resolutions. The dots indicate that there is at least one profile in a grid cell. Red circles schematically show the radii of influence of the three passes for the different resolutions during the objective analysis procedure (see text and Table 1).

objective analysis which is analogous to switching from a noneddy-resolving to an eddy-resolving model of ocean circulation (Malone et al., 2003; Oschlies, 2002).

Eddy-resolving ocean circulation models have consistently shown that the level of eddy kinetic energy in the Gulf Stream system is higher than the kinetic energy of the mean currents (e.g., Thoppil et al., 2011). It was also noted that mesoscale variability is integrated in the seasonal cycle of the large-scale currents, with a rather complicated interdependence (Kang et al., 2016; Rieck et al., 2015). Therefore, for the cumulative effects of mesoscale processes to be mapped properly, the seasonal signal should be fully resolved in the first place (Seidov et al., 2018).

4. Data Coverage and Signal-to-Noise Estimates

The central question regarding gridded data quality and reliability on different grids is how densely the grid cells are filled with observed data. In practice, it reduces to a ratio of the number of grid cells with data to the number of all cells in the region. Obviously, this ratio would be very different for the three implemented resolutions of 1° × 1°, 1/4° × 1/4°, and 1/10° × 1/10° when one cell of the 1° × 1° grid contains sixteen 1/4° × 1/4° cells and one hundred 1/10° × 1/10° cells. There is no effective way to compute mean (*MEAN*) and standard deviation (*STD*) for high-resolution grids that would be comparable to coarse-resolution values. In some extreme cases, those statistical measures may even become meaningless. For instance, if 100 observed profiles were regularly spaced across an idealized 1° × 1° grid cell, it would translate into a single profile in each of the 1/10° × 1/10° grid cells. Although simple descriptive statistics (MEAN and STD) in the hypothetical 1° × 1° grid cell with 100 evenly spaced profiles would be well attainable and meaningful, the statistics for each of the 100 cells of the 1/10° × 1/10° grid would yield just one profile for MEAN and no STD at all, thus rendering the simple statistics meaningless. Indeed, in the aforementioned idealized data distribution case, high-resolution mapping would have provided a detailed spatial temperature distribution across the imaginary 1° cell instead of just one number in the center of it, thus assuming homogeneity within the cell. For instance, if a hydrographic front of ~30 km width runs across a cell of the 1° × 1° grid, it would not be detected on such a coarse grid. On the contrary, if this front runs across the same 1° × 1° area but covered by a 1/10° × 1/10° grid, it would be seen. It should be noted that data coverage on finer-resolution grids, although still good in the NWA region, is far from uniform, and thus, there are many empty cells on the finer grids—far more if compared to the coarser 1° × 1° grid.

Figure 2 illustrates the data distribution for climatological July for the decade 1995–2004. All other decades (not shown) have comparable coverage. Each dot in Figure 2 represents a cell where at least one profile was observed during any July within the 1995–2004 decade for all three grids—1° × 1° (a), 1/4° × 1/4° (b), and 1/10° × 1/10° (c). We illustrate monthly rather than yearly or seasonal distributions because monthly data are the key for revealing mesoscale variability. The red circles in Figures 2a–2c show the radii of influence for the three passes of optimal interpolation varying from longer (coarse resolution) to shorter (fine resolution) lengths (see the numbers in Table 1). The difference between the radii of influence for the grids with different resolutions explains the structural disparities between fine- and coarse-resolution ocean mapping and respective climate analyses discussed in the following sections.

The total number of cells with water (i.e., excluding land and bottom) at 10-m depth is 864 (of total 1,320 cells, i.e., with the land and bottom cells included) on 1° × 1° grid, 14,174 (of 21,120 total) on 1/4° × 1/4°, and 89,873 (of 132,000 total) on 1/10° × 1/10°, respectively (showing almost perfect 1:16:100 ratio). Noticeably, with higher resolutions and smaller grid cells, a more accurate representation of the coastline and bottom topography is attained when compared to coarser resolutions. This increased areal coverage by ~3% on the 1/10° × 1/10° grid relative to the 1° × 1° grid.

Unsurprisingly, almost all cells on the 1° × 1° grid have data for a selected month regardless of the decade (Figure 2 illustrates the data distributions in climatological July for 1995–2004 on the three grids). In most cases, there are more than five profiles in a 1° cell, sometimes many more (see data distributions at https://www.nodc.noaa.gov/OC5/regional_climate/nwa-climate/). The data distribution on the 1/4° × 1/4° grid (Figure 2b) reveals somewhat sparser but still relatively good coverage. Finally, despite expectedly far more data gaps on 1/10° × 1/10° grid, the Gulf Stream region is well covered with most cells having at least one profile per climatological month for each decade. Since every 1° cell contains one hundred 1/10° cells, the data-rich regions along the coast appear as heavy-shaded areas in Figure 2c, with empty grid cells in many other places.

It is important to recall here that irregularly distributed observed data are mapped onto a regular grid using the objective analysis procedure that begins with a first-guess value of the parameter assigned to the center of each cell followed by three passes with decreasing radiuses of influence (see section 1 and Table 1). Two portions of the entire objective analysis process are critical for building high-resolution climatologies. First, the empty cells on higher resolutions are not "empty" anymore as they are filled with first-guess values before the objective analysis procedure begins. In both cases of 1/4° × 1/4° and 1/10° × 1/10° grids, the first-guess fields are simply the objectively analyzed values from the 1° × 1° grid (temperature, salinity, etc.). Second, the neighboring cells within the radius of influence are used to modify (through a weighting scheme) the first-guess values initially assigned to each cell, with a low-pass filter completing the procedure (see, e.g., Locarnini et al., 2013, for more information). In areas with little or no data on the finer-resolution grids, the 1° × 1° grid climatological field becomes the dominant signal as it is the first-guess field.

Also important, the climatic fields with empty cells on higher-resolution grids inherit the signal-to-noise ratio (S2N, discussed below) from the 1° × 1° grid. This becomes the baseline that can or cannot be further improved on finer grids depending on data availability.

In principle, one could have calculated S2N on 1° × 1° grid using the classical definition of S2N as the ratio of the MEAN to STD, that is, S2N = MEAN/STD (Smith, 2013). There is a caveat, though. The MEAN in the NWA region would change significantly from much colder water in the north to much warmer water in the south. This would provide a misrepresentation of the S2N because the signal is not necessarily higher in warmer water and lower in colder water. Therefore, regardless of the actual geographical distributions of MEAN values, the only real measure of the noise in such an inhomogeneus region would then be STD. The STD for each cell was calculated using the technique described in, for example, Locarnini et al. (2013) and can be used for assessing the noise level on any grid for any decade at any depth level for monthly, seasonal, or annual time periods (data available at https://www.nodc.noaa.gov/OC5/regional_climate/nwa-climate/).

Figure 3 presents the STD (i.e., the measure of variability) of monthly (here for July as an example) temperature at 10 m for the 1995–2004 decade on (a) 1° × 1°, (b) 1/4° × 1/4°, and (c) 1/10° × 1/10° grids. As might have been expected, STD is elevated in the Gulf Stream System area. What is less intuitive, the STD values on the finer grids are lower than on 1° × 1° grid. However, there are far more areas on finer grids where STD could not be computed because of data sparsity (black dots indicate cells with at least two profiles and where STD was calculated; white cells indicate where STD could not be calculated due to insufficient data). However, because the first-guess field for the finer grids is the objectively analyzed values from the 1° × 1° grid, the S2N in the cell without data on finer grids inherits the S2N from the coarser grid.

It is imperative to have a large S2N or, equivalently, small STD everywhere meaning the signal dominates the noise. Otherwise, any operation with a small S2N would be liable to the noise dominance over the signal. In regions with high variability, S2N is lower because STD is large regardless of MEAN. For example, in the subtropics, far from the Gulf Stream and other intense currents, the variability (and accordingly STD) of temperature and salinity is lower than the vicinity of such currents allowing for a small STD and large S2N.
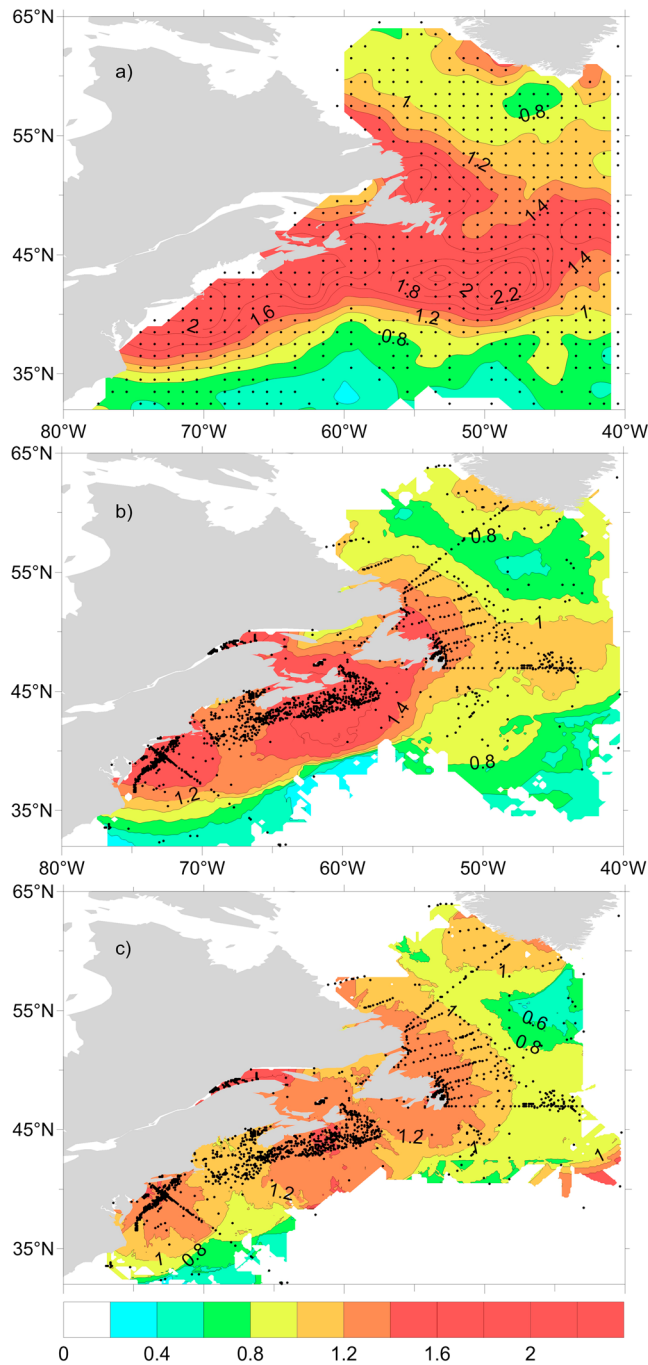
Figure 3. (a–c) Standard deviation of seawater temperature at 10-m depth for July 1994–2004. Only data points with two or more profiles are plotted (i.e., where standard deviation can be computed).

In contrast, STD is greater in the frontal zones where the temperature changes rapidly across the front and the jet meanders. In such dynamic areas, S2N is expectedly low because STD is large.

The analysis of STD distribution on different grids provided in Figure 3 indicates that the STD (S2N) is greater (lower) on the 1° × 1° grid compared to the finer grids. The greater (lower) STD (S2N) values on coarser grids result from higher variability across the larger cells, whereas finer-resolution cells would have a smaller (larger) STD (S2N) due to lower variability of the measured data within the smaller cells. Consider the idealization with uniform data distribution (e.g., 100 profiles) across a 1° cell with temperature and salinity varying between 10 and 24 °C. The STD of the data within that cell would be quite large. On the other hand, in a single 1/10° cell within that 1° cell, there would be more homogeneous temperature and salinity translating into a smaller STD in each cell on the finer-resolution grid and, consequently, a higher S2N ratio.

As seen in Table 1 and Figure 2, the radius of influence varies during the three successive passes of the objective analysis. It begins with a range of 892 to 446 km in the coarse-resolution grid of 1° × 1° to the range of 321 to 214 for 1/4° × 1/4° grid and finally to the range of 253 to just 154 km on the finest grid with 1/10° × 1/10° resolution. Thus, the radius of influence at the end of the three passes on 1/10° × 1/10° grid resolution is 30% shorter than on 1/4° × 1/4° and nearly 3 times—300%—shorter than on 1° × 1° grid. In a crude analogy to numerical models, the shortening of the radius of influence could be seen as decreasing the role of lateral turbulent mixing (or eddy diffusion) in eddy-resolving models (Kantha & Clayson, 2000).

The decision on whether to use eddy-permitting or eddy-resolving mapping in any region with sufficient data is a trade-off between eddy-resolving mapping on the 1/10° × 1/10° grid with many empty cells filled by the objective analysis and eddy-permitting mapping on the 1/4° × 1/4° grid with fewer empty cells filled by objective analysis but with less detailed representation which could miss important mesoscale elements.

5. NWARC Applications

5.1. NWARC Ocean Climate Applications

One of the major goals of data-based ocean climate mapping is to support ocean and climate studies. Since the ocean has a much larger heat capacity than the atmosphere and land, climate change on decadal and longer timescales is therefore strongly controlled by the ocean. Water temperature and corresponding ocean heat content averaged over ~30-year periods (considered a "climate normal" by the World Meteorological Organization, WMO, 2011) would then be the most meaningful definition of the ocean climate. Thus, analyzing oceanic climate changes (or more accurately *climate shifts*) can be done by examining the temperature and heat content differences between two consecutive ~30-year intervals.

Figure 4 illustrates the superiority of higher spatial resolutions by showing January decadal temperature (left column) and salinity (right column) at 50 m in the NWA for the decade of 1985–1994 with three grid resolutions: (a, b) 1° × 1°, (c, d) 1/4° × 1/4°, and (e, f) 1/10° × 1/10°. Figures 4a and 4b depict a coarse-resolution representation of the Gulf Stream dynamics reflected in the temperature and salinity structure. On a coarse-resolution grid, many of the essential characteristics of this system (e.g., the width of the jet, separation from the coast, intensity of the frontal zone, and the area occupied by the cold Slope Water Current) are not
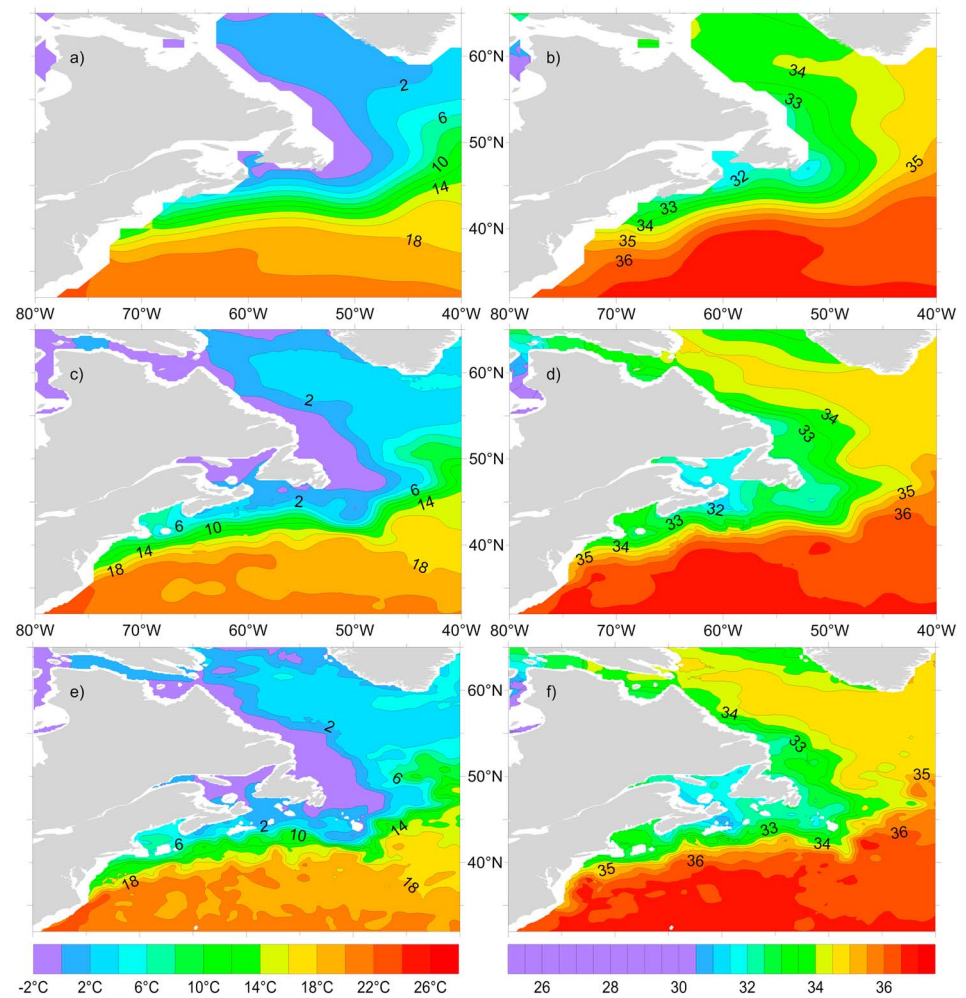
Figure 4. The 1985–1994 January objectively analyzed seawater temperature (left column) and salinity (right column) at 50-m depth on the grids with: (a, b) 1° × 1°, (c, d) 1/4° × 1/4°, and (e, f) 1/10° × 1/10° resolutions.

correctly replicated. On the contrary, the high-resolution regional climatologies on 1/4° × 1/4° (Figures 4c and 4d) and 1/10° × 1/10° (Figures 4e and 4f) grids reveal many of these important details not seen in Figures 4a and 4b.

A more detailed climatology is important for diagnosing ocean climate change, quite similar to ocean circulation modeling, when not only are the finer details of the circulation seen in the calculations but the calculations themselves become more accurate and physically consistent. For example, only eddy-resolving ocean models with much finer (at least 6 times finer) resolution when compared to the traditional 1° resolution ocean models solved the problem of correctly representing the Gulf Stream separation from the coast within the Cape Hatteras vicinity (e.g., Chao et al., 1996). Even grid resolutions which are 6 to 10 times finer than a 1° grid are not fully satisfactory for simulating all the details of the Gulf Stream separation (Ezer, 2016). With 1/10° × 1/10° resolution, we are approaching the accuracy needed for properly detailing this important feature, which is not possible on coarser grids.

Although the 1/4° × 1/4° fields (Figures 4c and 4d) are improved over the 1° × 1° fields, they are still somewhat oversmoothed when compared to the results of eddy-resolving models (i.e., Barnier et al., 2014; Chao et al., 1996; Maze et al., 2013; Treguier et al., 2005). The 1/10° × 1/10° mapping (Figures 4e and 4f) reveals a better structured Gulf Stream system comparable to what is seen in eddy-resolving models and satellite images (e.g., Andres, 2016; Barnier et al., 2014; Kelly et al., 2010; Madec, 2008; Treguier et al., 2017; Zhai & Greatbatch, 2006). Importantly, both 1/4° × 1/4° and 1/10° × 1/10° grids show very different temperature
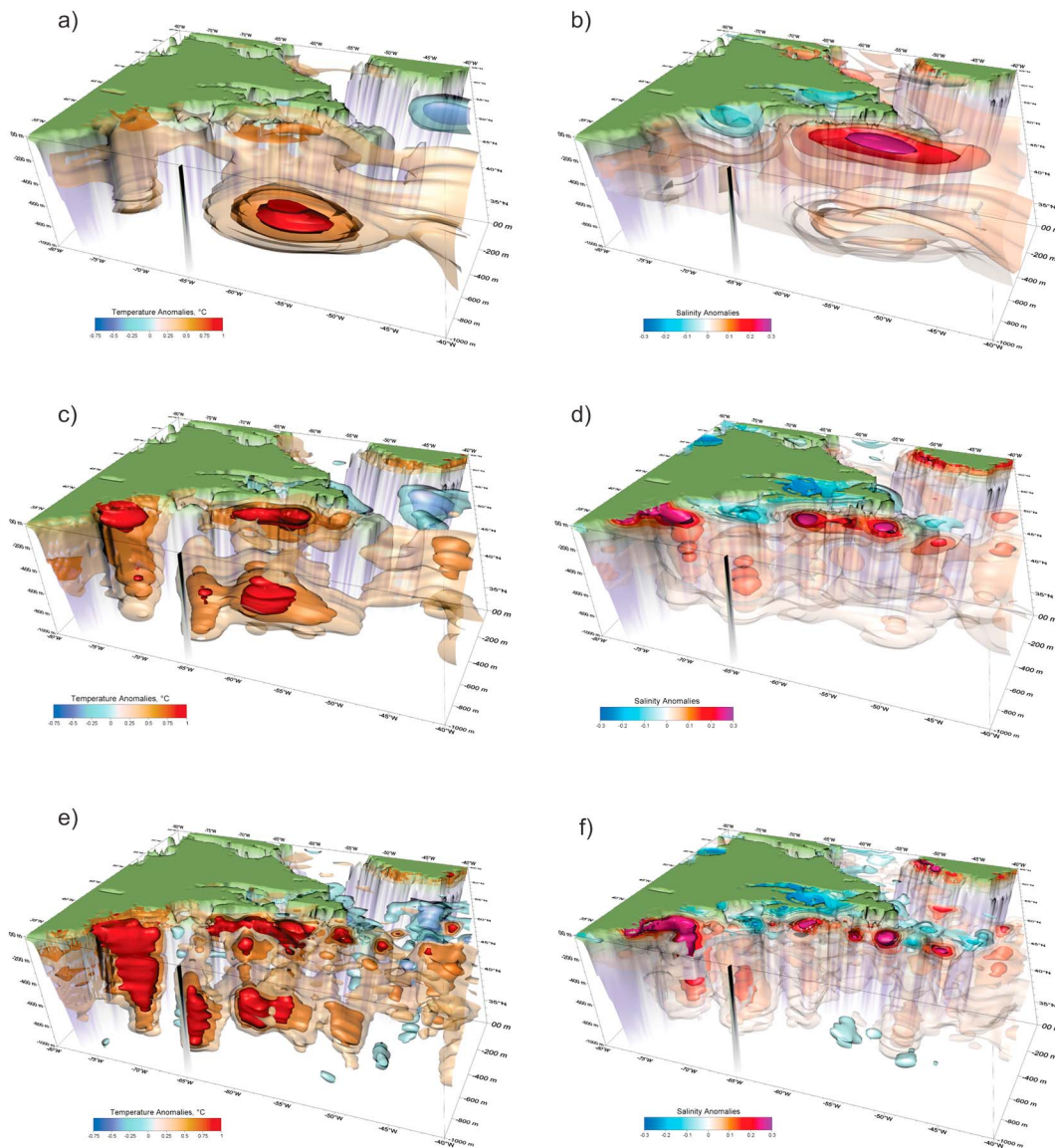
Figure 5. Seawater temperature and salinity anomalies between two 30-year ocean climates (1985–2012 minus 1955–1984) within the Northwest Atlantic domain (80°W to 40°W, 32°N to 65°N) over the 0- to 1,000-m depth layer on the grids with (a, b) 1° × 1°, (c, d) 1/4° × 1/4°, and (e, f) 1/10° × 1/10° resolution. The isothermal surfaces of $\Delta T = -0.5$, -0.25, 0.5, 0.75, and 1 °C and isohalines surfaces of $\Delta S = -0.5$, -0.25, 0.5, 0.75, and 1 are shown by different colors.

and salinity fields when compared to the 1° × 1° grid, while the fields on the 1/10° × 1/10° grid are closer to the 1/4° × 1/4° fields than the 1° × 1° fields.

5.2. Decadal Ocean Climate Variability and ~30-Year Ocean Climate Shift

Ocean climate shift can be assessed by ocean temperature and heat content differences between two consecutive ~30-year periods. Using WOA13 on 1/4° × 1/4° grid, Seidov et al. (2017) showed that the heat is accumulated in the NA heterogeneously, with the strongest heat gain in the ~30-year (1985–2012 minus 1955–1984) climate shift found in the subsurface layers south of the Gulf Stream System. A detailed view of the western part of the NA suggested that this heat gain occurred in two layers of water. Applying this analysis for the NWA region using NWARC, we found an even more complex heat gain pattern mapped on the 1/10° × 1/10° grid resolution. Figure 5 demonstrates the ~30-year climate shift in seawater tempera-ture and salinity between the multidecadal periods of 1955–1984 and 1985–2012 within the NWA domain on the (a, b) 1° × 1°, (c, d), 1/4° × 1/4°, and (e, f) 1/10° × 1/10° spatial resolutions. Both heat and salt are
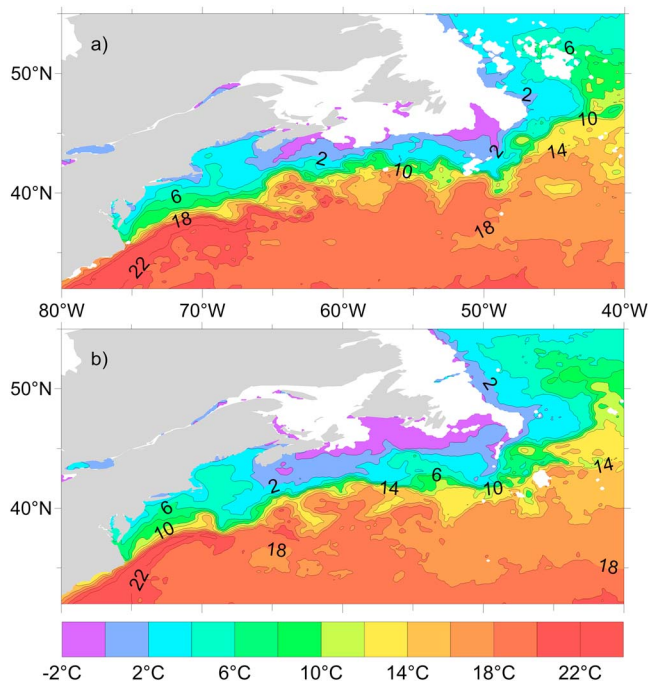
Figure 6. Monthly sea surface temperature in the Gulf Stream area: (a) March 2003 and (b) March 2007 from the Moderate-resolution Imaging Spectroradiometer-Aqua acquired from http://apdrc.soest.hawaii.edu:80/dods/public_data/satellite_product/MODIS_Aqua/9km_sst4.

gained in the 30-year shift, with these gains occurring mostly south and southeast of the Gulf Stream. Additionally, both eddy-permitting and eddy-resolving analyses suggest a substantial heat and salt gain in the vicinity of the Gulf Stream separation from the coast near Cape Hatteras, which cannot be resolved in the coarse-resolution analysis. There is a much stronger heat gain in the upper 300 m of the southeastern Gulf Stream vicinity than in the coarse-resolution mapping (compare Figures 5a, 5c, and 5e).

Coarse-resolution analysis provides an oversimplified pattern of temperature and salinity fields with one generalized body of warmer water (Figure 5a) and one body of saltier water (Figure 5b). While it is expected that temperature and salinity changes will be density compensating (e.g., warming with salinification and cooling with freshening), this is not always true in the NWA. Salinity changes at the sea surface are mainly controlled by air-sea freshwater exchange and ocean advection, while surface temperature is primarily controlled by air-sea heat exchange. Therefore, the temperature and salinity climate shifts do not always correlate and the cores of salt accumulation (or loss) do not always coincide with the cores of heat gain (or loss) as seen in distinct areas of strong freshening north of the Gulf Stream without corresponding cooling (Figures 5b, 5d, and 5f). Moreover, the regions of heat and salt gains are not completely coincidental—the warmer regions are within the upper 200 m and between 300 and 700 m, while the salt gains occur closer to the surface (compare Figures 5c and 5d and 5e and 5f). In contrast, the heat and salt gains near the Gulf Stream separation do coincide but with the heat gain penetrating much deeper than the salt gain. The area occupied by the Slope Water freshens without any significant warming or cooling.

The ocean heat content (OHC) distribution is generally consistent with temperature distributions (i.e., as the water temperature changes, the OHC follows). Multiple studies have found that the strongest OHC changes over the last half century have occurred in the NA (Boyer et al., 2007; Levitus et al., 2012; Lozier et al., 2008). The changes in OHC have been analyzed in numerous studies (Chafik et al., 2016; Cheng et al., 2016; Domingues et al., 2008; Giese et al., 2016; Häkkinen et al., 2016; Williams et al., 2015; Willis et al., 2004), inferred from climate models (Cheng et al., 2016; Desbruyères et al., 2015), and diagnosed through reanalysis efforts (Balmaseda et al., 2013; Carton & Santorelli, 2008; Häkkinen et al., 2015; Palmer et al., 2015). The NA decadal OHC variability and its connection to the Atlantic Multidecadal Oscillation have been discussed in Seidov et al. (2017). As Figures 5a, 5c, and 5e suggest, the character of heat accumulation on finer grids differs radically from that on the coarser one. Like the ~30-year temperature differences, the OHC analysis on the coarse-resolution grid is too general and does not reflect the mesoscale features of the OHC variability.

5.3. Comparison With Satellite Snapshots of Mesoscale Variability

Repetitiveness or stochastic periodicity of the major elements of mesoscale processes in the Gulf Stream system is seen in high-resolution in situ climatologies, satellite images (Kelly et al., 2010), and eddy-resolving models (Barnier et al., 2014). To illustrate the presence of the repetitive mesoscale disturbances in remotely sensed sea surface temperature (SST), two March snapshots, separated by 4 years, similar to the snapshots depicted in Kelly et al. (2010), are analyzed in Figure 6. Comparing Kelly et al. (2010) and Figure 6, there are clearly seen repeating filaments with comparable amplitudes appearing in nearly the same places even though the monthly snapshots are separated by four years. The monthly SST data are from the Moderate-resolution Imaging Spectroradiometer onboard the Aqua satellite. We used the midinfrared (4 μm) monthly SST data with a horizontal resolution of ~9 km acquired from http://apdrc.soest.hawaii.edu/dods/public_data/satellite_product/MODIS_Aqua/9km_sst4 (OBPG, 2015; Werdell et al., 2013).

To reaffirm the contention that repetitive mesoscale patterns can be seen in decadal climatologies, near-surface NWARC and surface satellite-based monthly decadal climatologies are compared side by side. Figure 7 shows three sets of decadal October temperature maps from NWARC (left column) on the
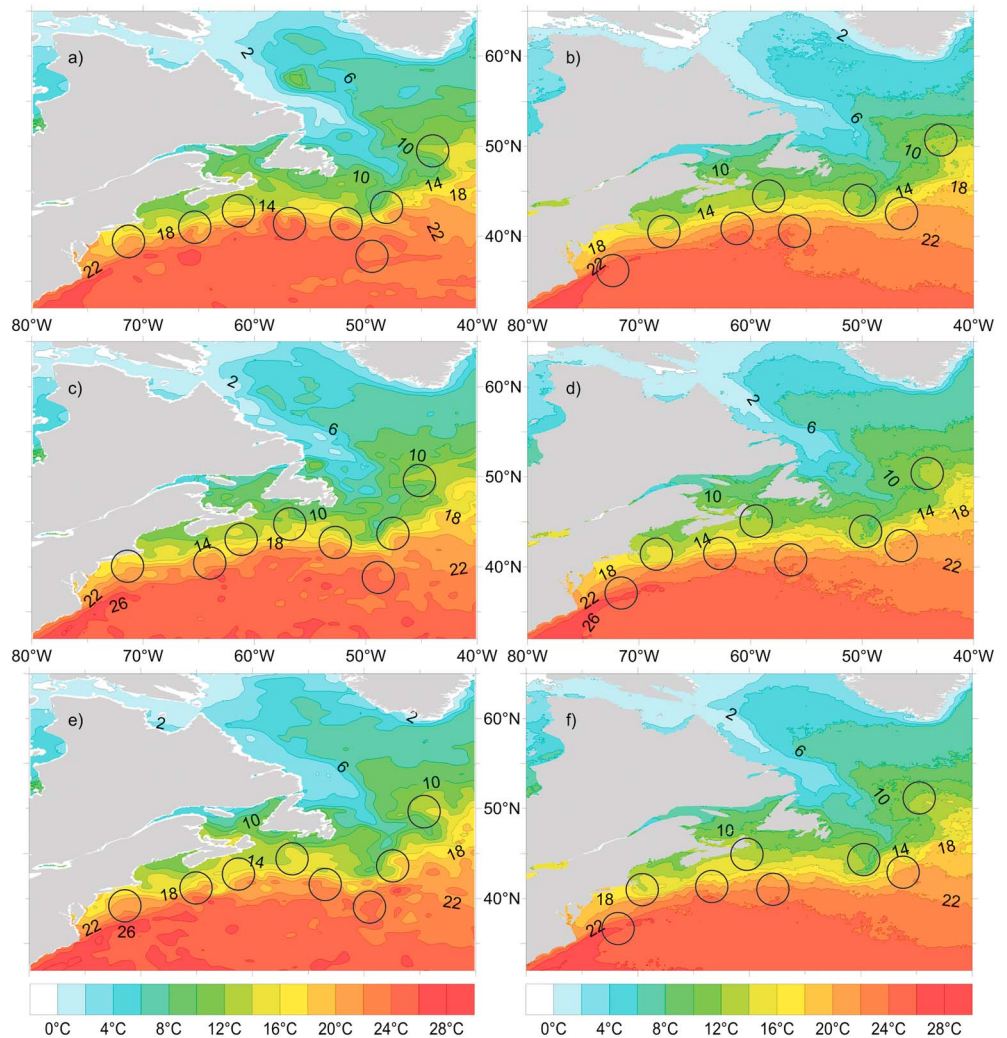
Figure 7. October seawater temperature from Northwest Atlantic regional climatology at 10-m depth (left column) and sea surface temperature from AVHRR Pathfinder satellite observations (right column) for the decades: (a, b) 1985–1994, (c, d) 1995–2004, and (e, f) 2005–2012. Examples of repetitive filaments in the Gulf Stream area are denoted by the black circles.

1/10° × 1/10° grid at 10 m and satellite decadal October SSTs (~4-km resolution) computed using the Advanced Very High Resolution Radiometer (AVHRR) Pathfinder Version 5.2 data (right column) for the decades 1985–1994, 1995–2004, and 2005–2012. Similar to the two individual monthly snapshots in Figure 6, repetitive mesoscale features can be seen in Figure 7 (some of the meanders, squirts, and filaments are marked by black circles for easier spotting). Both NWARC and satellite-based ocean surface (or near-surface) mapping are consistent with the hypothesis that mesoscale variability is interlocked with the seasonal cycle and that there is a great deal of repetitiveness of specific patterns surrounding unstable jet currents, especially the Gulf Stream and its extension (e.g., (Kelly et al., 2010)).

5.4. Eighteen Degree Water and Subtropical Water Heaving

Since temperature and salinity fields show similar tendencies in the core of the subtropical gyre (Figure 5), one may argue that subtropical water heaving could be the cause of the warming/salinization in the subtropical gyre, at least to some extent. This heaving, presumably instigated by a long-term wind stress pattern change (Huang, 2015; Lozier et al., 2008), was noticed in the analysis of the NA climate change based on WOA13 data with 1/4° × 1/4° grid resolution (Huang, 2015; Seidov et al., 2017).

Since subtropical water heaving is seen as a possible cause of localized heat trapping on multidecadal time-scales, the geography of the gain-trapping pockets from in situ climatological mapping is important. According to Seidov et al. (2017) and Figure 5, the highest rates of heat and salt gain occur in the Sargasso Sea, southeast of the Gulf Stream path in the region occupied by the Atlantic Mode Water, also known as the Subtropical Mode Water or the Eighteen Degree Water (EDW; Hanawa & Talley, 2001; Joyce, 2012; McCartney & Talley, 1982; Worthington, 1976). Some authors argue that the maximum heat gain below 200-m southeast of the Gulf Stream could be caused by the vertical displacement of isopycnal surfaces constituting the EDW heaving (e.g., Bindoff & McDougall, 1994; Häkkinen et al., 2015, 2016). The assumption that the subtropical heat gain in the Gulf Stream System is linked to EDW variability has existed for quite some time (Hanawa & Talley, 2001; McCartney & Talley, 1982; Worthington, 1976). It has been argued that EDW can store large amounts of heat through expansion and discharge large amounts of heat through contraction over time periods of several years to decades (Kelly & Dong, 2013) and that there is a strong positive correlation between the volume of EDW and the heat content of the EDW layer (Kwon & Riser, 2004; see their Figures 2b and 2d).

The assumed interplay of the EDW and OHC in the NA implies that the volume of EDW depends on the interaction between Ekman pumping, heat fluxes across the surface, and heat advection within the Gulf Stream and in the subtropical recirculation gyre (Dong & Kelly, 2004; Kelly & Dong, 2004, 2013; Seidov et al., 2017). Additionally, a combination of warm subtropical water heaving and the apparent AMOC slowdown (e.g., Bryden et al., 2005; Cunningham et al., 2013; Smeed et al., 2014) may be responsible for the excessive heat accumulation in the Gulf Stream System and that the heat and salt anomalies buildup can be rather patchy because of the high level of mesoscale dynamics in this region. However, we emphasize that comparing observed long-term changes of AMOC with changes in observed OHC should be done cautiously because the observations of each may not be from the same years and/or the same seasons. Therefore, we cannot prove or disprove this hypothesis, but we do believe that it could be a reasonable explanation worthy of future exploration.

With in situ decadal ocean mapping, an enhanced ocean climate shift below 300-m depth southeast of the Gulf Stream approximately within the EDW area is evident in Figure 5 (see also Figures 1 and S1 in Seidov et al., 2017). It is tempting to attribute, at least partially, this strong and localized subsurface warming to vertical migration ("heaving") of isopycnal surfaces (Bindoff & McDougall, 1994; Häkkinen et al., 2015, 2016). Lozier et al. (2008) showed the role of the curl of wind stress in deepening the thermocline in the subtropical NA (which now is termed by many as *heaving*). In turn, Seidov et al. (2017) argued that heat accumulation follows SST anomalies created by large-scale, long-term ocean-atmosphere heat exchange which is then followed by wind-induced heaving of warm water. This is in line with the finding that increased EDW volume leads to EDW heat content increase (Kwon & Riser, 2004). Moreover, an increase in the volume of EDW leads to an increase in OHC which should coincide with increased salinity over long periods of time.

To illustrate how long-term changes of temperature in the subtropical NWA may be indicative of EDW heaving, the depths of EDW for two ~30-year intervals and their differences were computed and analyzed in conjunction with the changes of the curl of wind stress and related Ekman pumping over the comparable time interval. Figure 8 shows the depths of EDW (in meters) for two ~30-year intervals, 1955–1984 (Figures 8a– 8c) and 1985–2012 (Figures 8d–8f), and the EDW's depths differences between those two ~30-year intervals (Figures 8g–8i; note the different color scales for the depths and depth differences). It is clear that the differences in grid resolution do matter for mapping EDW depth as the comparison between the depths and their differences for the three grids—1° × 1°, 1/4° × 1/4°, and 1/10° × 1/10° (left, middle, and right columns, respectively) can be clearly seen. EDW depths and their differences on the coarse-resolution grid (Figures 8a, 8d, and 8g) illustrate smooth EDW depth distributions and EDW heaving, while the finer-resolution grids provide a more detailed picture and are consistent with strong mesoscale variability southeast of the Gulf Stream.

The ~30-year climate shift in the EDW depth in Figure 8 is compared with the Ekman pumping change (wind stress curl serves as a proxy) over approximately the same period. The wind stress curl was computed using the wind stress data from Carton and Giese (2008) on 1/2° × 1/2° grid (see the data source at http://apdrc. soest.hawaii.edu/dods/public_data/SODA/soda_pop2.2.4.info). The wind stress curl for the period 1955–2010 is shown in Figure 9a, with the wind stress vectors superimposed on the wind stress curl map. The areas of positive wind stress curl show where vertical Ekman velocities are upward, while the regions with negative
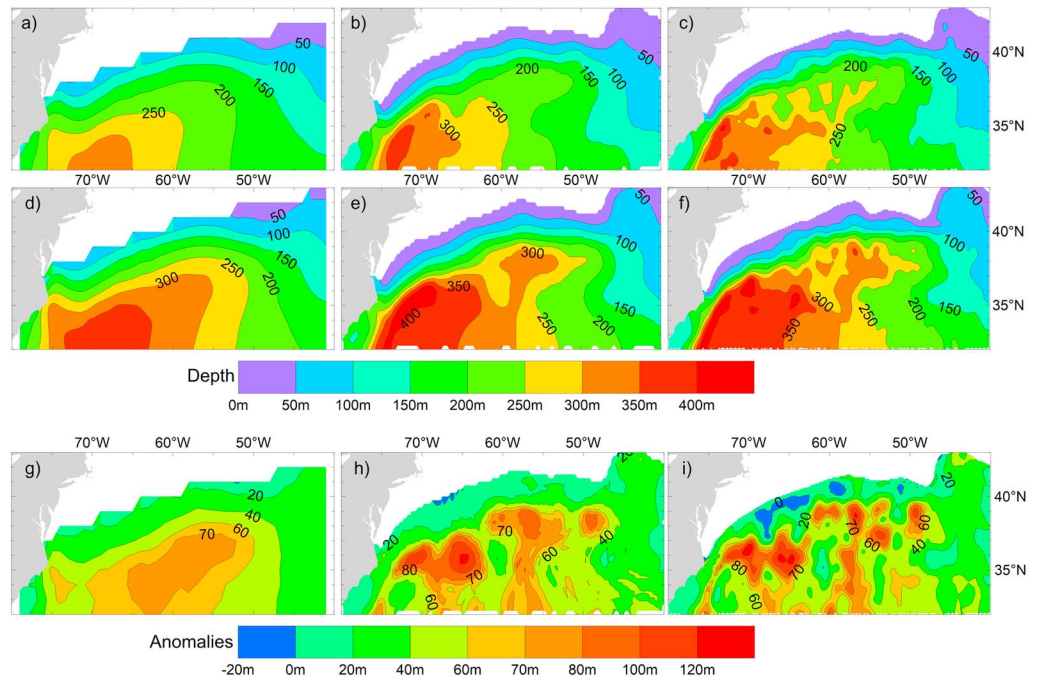
Figure 8. Depths of the Eighteen Degree Water for the decades: (a–c) 1955–1984 and (d–f) 1985–2012 and differences of Eighteen Degree Water 's depths (1985–2012 minus 1955–1984) between those two periods (g–i) on the grids with 1° × 1° (a, d, g), 1/4° × 1/4° (b, e, h), and 1/10° × 1/10° (c, f, i) resolutions. The color scales for depths (a–f) and the 30-year differences of the depths (g–i) are different.

values of wind stress curl are the regions of downward Ekman velocities. The climatic shift of the wind stress curl between 1985–2010 and 1955–1984 is displayed in Figure 9b. The areas with negative values of the climate shift in Ekman pumping signify slowing upward or increasing downward Ekman velocities, and the positive values indicate the opposite.

The change in the EDW depths (Figures 8g– 8i) compares quite well with the climatic shift of Ekman pumping velocities between the years 1985–2010 and 1955–1984 as shown in Figure 9b. As Figures 8 and 9b reveal, both on 1/4° × 1/4° and 1/10° × 1/10° grids (middle and right columns in Figure 8), the EDW depth change
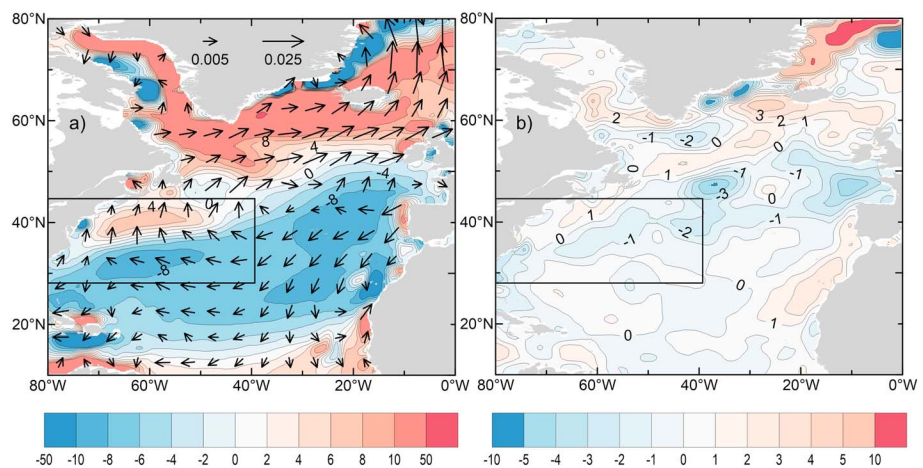
Figure 9. (a) Wind stress curl (10–7 Nm^{-3}, shaded) and wind stress (Nm^{-2}, vectors) over the 1955–2010 time period and (b) the differences of the wind stress curl (10–7 Nm^{-3}, shaded) between 1985–2010 and 1955–1984. Black rectangles show the area where the Eighteen Degree Water depths are plotted in Figure 8. Wind stress adopted on 1/2° × 1/2° grid from Carton and Giese (2008); data at http://apdrc.soest.hawaii.edu/dods/public_data/SODA/soda_pop2.2.4.info.

closely reflects the ~30-year climate shift in the Ekman vertical velocity pattern (Figure 9b). The regions where the EDW deepens coincide closely with the areas of negative vertical Ekman velocities indicating stronger sinking motion. Although the curl of wind stress is not at an eddy-resolving resolution from the ocean perspective, it is close to the eddy-permitting resolution of 1/4° × 1/4° which gives it a closer resemblance to the eddy-permitting EDW depths and their climatic shifts than eddy-resolving maps (Figures 8b, 8e, and 8h and 9b). Comparison of the EDW heaving with the ~30-year shift of the wind stress curl (and consequently Ekman pumping) reveals a strong resemblance of the eddy-permitting and eddy-resolving EDW heaving patterns with two major cores of heat accumulation. In contrast, the EDW heaving pattern on 1° × 1° grid (Figures 8a, 8d, and 8g) does not match the ~30-year Ekman pumping shift and therefore does not reflect the localized nature of EDW heaving.

Another contributing factor of heat accumulation in the subtropical part of the NWA could be the slowing of AMOC's upper limb—the Gulf Stream and its extension (Bryden et al., 2005; Kelly et al., 2016; Smeed et al., 2014). It can be argued that the fast accumulation of OHC in the subtropical southwestern NA may result from a combination of the AMOC slowing and wind-induced subtropical water heaving (Seidov et al., 2017). However, without dismissing a possible role of the AMOC in the EDW long-term variability, comparing the wind-stress and EDW heaving patterns (Figures 8 and 9) confirms that the wind stress is most probably the lead factor in subtropical subsurface water warming.

6. Discussion and Conclusions

The major advantage of in situ mapping of ocean temperature and salinity on regular grids with resolution matching eddy-permitting and even eddy-resolving ocean circulation models is that it yields regional ocean climatologies qualitatively and quantitatively superior to ones with coarser resolution. An important inference from analyzing eddy-resolving ocean climatologies is that the stochastically repetitive mesoscale variability in dynamically active regions preserves repeated mesoscale dynamics in the decadal tracer fields. Comparison of high-resolution in situ ocean mapping of near-surface temperature with the climatologies computed from satellite SST supports our hypothesis that the *seasonal signal carries the superimposed repetitive mesoscale signals and thus decadal climatologies—monthly, seasonal, and annual—reflect the cumulative effect of mesoscale dynamics on mapping of the large-scale regional ocean climate state and variability*. Eddy-permitting and eddy-resolving in situ mappings both retain this cumulative effect of mesoscale dynamics in gridded thermohaline fields computed using in situ observations with the eddy-resolving climatologies on the 1/10° × 1/10° resolution more accurately depicting them, especially in the Gulf Stream vicinity. The most important conclusion is that eddy-permitting and eddy-resolving mappings do retain some mesoscale elements of the large-scale thermohaline fields (i.e., sharp frontal zones, jet meanderings, mesoscale filaments, and eddies), while the noneddy-permitting mapping does not show any trace of these phenomena.

The stochastic nature of repeating mesoscale elements within the tracer fields does not necessarily mean that, for example, the March synoptic and mesoscale pattern of temperature for one decade would most closely match the pattern for March of another decade; it might more closely resemble February or April of a different decade instead (or any time between February and April for that matter). However, the mesoscale variability is unmistakably repetitive within the seasonal cycles in all six decades.

The role of the changes in wind stress curl over the NA in ocean heat content accumulation was assessed in all three NWA regional climatologies—the coarse resolution, eddy permitting, and eddy resolving. The ~30-year climatic shift of the wind stress curl and related Ekman pumping most likely play a leading role in subsurface ocean heat accumulation in the region southeast of the Gulf Stream (east of the Gulf Stream separation from the coast at Cape Hatteras) although ocean-air heat exchange and advection within the Gulf Stream and recirculation are also important (Kelly & Dong, 2004). The heat accumulation or loss works through the EDW heaving induced by Ekman pumping. Although this, by itself, is not new and was proposed and discussed in a number of studies (Bindoff & McDougall, 1994; Häkkinen et al., 2016; Lozier et al., 2017), we contribute by showing that eddy-permitting mapping of the wind stress curl based on SODA v2.2.4 (Carton & Giese, 2008) correlates with the EDW heaving revealed in the ~30-year temperature differences from NWARC's eddy-permitting and eddy-resolving mapped temperature fields. It also demonstrated that a noneddy-permitting climatology (NWARC with the 1° × 1° resolution) departs from the wind stress curl patterns.

To summarize, the high-resolution climatologies of the NWA Ocean can be instrumental in detailing the regional descriptions of ongoing global ocean climate change, long-term variability, and trends. It also supports the case for using eddy-permitting resolution climatologies, with eddy-resolving climatologies desired in regions with dense data distributions (as in the coastal zone along the east coast of the United States and Canada). In a more general framework, NCEI's collection of regional ocean climatologies may help to better connect data processing and investigative efforts in the realm of regional oceanography.

References

Andres, M. (2016). On the recent destabilization of the Gulf Stream path downstream of Cape Hatteras. *Geophysical Research Letters*, *43*, 9836–9842. https://doi.org/10.1002/2016GL069966

Balmaseda, M. A., Trenberth, K. E., & Källén, E. (2013). Distinctive climate signals in reanalysis of global ocean heat content. *Geophysical Research Letters*, *40*, 1754–1759. https://doi.org/10.1002/grl.50382

Barnes, S. L. (1973). Mesoscale objective map analysis using weighted time series observations. In *NOAA Technical Memorandum ERL NSSL-62*, (60pp.). Washington, DC: NTIS.

Barnier, B., Blaker, A. T., Biatosch, A., Böning, C. W., Coward, A., Deshayes, J., et al. (2014). DRAKKAR: Developing high resolution ocean components for European Earth system models. *CLIVAR Exchange*, *65-19*(2), 18–21.

Bindoff, N. L., & McDougall, T. J. (1994). Diagnosing climate change and ocean ventilation using hydrographic data. *Journal of Physical Oceanography*, *24*(6), 1137–1152. https://doi.org/10.1175/1520-0485(1994)024<1137:DCCAOV>2.0.CO;2

Bower, A. S., Rossby, H. T., & Lillibridge, J. L. (1985). The Gulf Stream—Barrier or blender? *Journal of Physical Oceanography*, *15*(1), 24–32. https://doi.org/10.1175/1520-0485(1985)015<0024:tgsob>2.0.co;2

Boyer, T., Levitus, S., Antonov, J., Locarnini, R., Mishonov, A., Garcia, H., & Josey, S. A. (2007). Changes in freshwater content in the North Atlantic Ocean 1955–2006. *Geophysical Research Letters*, *34*, L16603. https://doi.org/10.1029/2007GL030126

Boyer, T., Levitus, S., Garcia, H., Locarnini, R. A., Stephens, C., & Antonov, J. (2005). Objective analyses of annual, seasonal, and monthly temperature and salinity for the World Ocean on a 0.25° grid. *International Journal of Climatology*, *25*(7), 931–945. https://doi.org/10.1002/joc.1173

Boyer, T. P., Garcia, H. E., Locarnini, R. A., Zweng, M. M., Mishonov, A. V., Reagan, J. R. (2014). 2013 World Ocean Atlas Aids High-Resolution Climate Studies. *Eos, Transactions American Geophysical Union*, *95*(41), 369–370. https://doi.org/10.1002/2014EO410002

Bryden, H. L., Longworth, H. R., & Cunningham, S. A. (2005). Slowing of the Atlantic meridional overturning circulation at 25°N. *Nature*, *438*(7068), 655–657. https://doi.org/10.1038/nature04385

Buckley, M. W., & Marshall, J. (2016). Observations, inferences, and mechanisms of Atlantic Meridional Overturning Circulation variability: A review. *Reviews of Geophysics*, *54*, 5–63. https://doi.org/10.1002/2015RG000493

Carton, J. A., & Giese, B. S. (2008). A reanalysis of ocean climate using simple ocean data assimilation (SODA). *Monthly Weather Review*, *136*(8), 2999–3017. https://doi.org/10.1175/2007MWR1978.1

Carton, J. A., & Santorelli, A. (2008). Global decadal upper-ocean heat content as viewed in nine analyses. *Journal of Climate*, *21*(22), 6015–6035. https://doi.org/10.1175/2008JCLI2489.1

Chafik, L., Häkkinen, S., England, M. H., Carton, J. A., Nigam, S., Ruiz-Barradas, A., et al. (2016). Global linkages originating from decadal oceanic variability in the subpolar North Atlantic. *Geophysical Research Letters*, *43*, 10,909–10,919. https://doi.org/10.1002/2016GL071134

Chao, Y., Gangopadhyay, A., Bryan, F. O., & Holland, W. R. (1996). Modeling the Gulf Stream System: How far from reality? *Geophysical Research Letters*, *23*(22), 3155–3158. https://doi.org/10.1029/96GL03003

Chapman, C., & Sallée, J.-B. (2017). Can we reconstruct mean and eddy fluxes from Argo floats? *Ocean Modelling*, *120*, 83–100. https://doi.org/10.1016/j.ocemod.2017.10.004

Cheng, L., Trenberth, K. E., Palmer, M. D., Zhu, J., & Abraham, J. P. (2016). Observed and simulated full-depth ocean heat content changes for 1970-2005. *Ocean Science Discussions*, *2016*, 1–21. https://doi.org/10.5194/os-2016-16

Cornillon, P. (1986). The effect of the New England seamounts on gulf stream meandering as observed from satellite IR imagery. *Journal of Physical Oceanography*, *16*(2), 386–389. https://doi.org/10.1175/1520-0485(1986)016<0386:Teotne>2.0.Co;2

Cunningham, S. A., Roberts, C. D., Frajka-Williams, E., Johns, W. E., Hobbs, W., Palmer, M. D., et al. (2013). Atlantic meridional overturning circulation slowdown cooled the subtropical ocean. *Geophysical Research Letters*, *40*, 6202–6207. https://doi.org/10.1002/2013GL058464

Cushman-Roisin, B., & Tang, B. (1990). Geostrophic turbulence and emergence of eddies beyond the radius of deformation. *Journal of Physical Oceanography*, *20*(1), 97–113. https://doi.org/10.1175/1520-0485(1990)020<0097:Gtaeoe>2.0.Co;2

Desbruyères, D., Mercier, H., & Thierry, V. (2015). On the mechanisms behind decadal heat content changes in the eastern subpolar gyre. *Progress in Oceanography*, *132*, 262–272. https://doi.org/10.1016/j.pocean.2014.02.005

Domingues, C. M., Church, J. A., White, N. J., Gleckler, P. J., Wijffels, S. E., Barker, P. M., & Dunn, J. R. (2008). Improved estimates of upper-ocean warming and multi-decadal sea-level rise. *Nature*, *453*(7198), 1090–1093. https://doi.org/10.1038/nature07080

Dong, S., & Kelly, K. A. (2004). Heat budget in the Gulf stream region: The importance of heat storage and advection. *Journal of Physical Oceanography*, *34*(5), 1214–1231. https://doi.org/10.1175/1520-0485(2004)034<1214:HBITGS>2.0.CO;2

Ezer, T. (2016). Revisiting the problem of the Gulf stream separation: On the representation of topography in ocean models with different types of vertical grids. *Ocean Modelling*, *104*, 15–27. https://doi.org/10.1016/j.ocemod.2016.05.008

Fofonoff, N. P. (1980). The Gulf Stream. In B. A. Warren & C. Wunsch (Eds.), *Evolution of physical oceanography: Scientific surveys in honor of Henry Stommel* (pp. 112–139). Cambridge, MA: MIT Press.

Fuglister, F. C. (1963). Gulf stream '60. *Progress in Oceanography*, *1*, 265–373. https://doi.org/10.1016/0079-6611(63)90007-7

Giese, B. S., Seidel, H. F., Compo, G. P., & Sardeshmukh, P. D. (2016). An ensemble of ocean reanalyses for 1815–2013 with sparse observational input. *Journal of Geophysical Research: Oceans*, *121*, 6891–6910. https://doi.org/10.1002/2016JC012079

Gill, A. E. (1982). *Atmosphere-ocean dynamics*. New York: Academic Press.

Gula, J., Molemaker, M. J., & McWilliams, J. C. (2016). Submesoscale dynamics of a Gulf Stream frontal eddy in the South Atlantic Bight. *Journal of Physical Oceanography*, *46*(1), 305–325. https://doi.org/10.1175/JPO-D-14-0258.1

Häkkinen, S., Rhines, P. B., & Worthen, D. L. (2015). Heat content variability in the North Atlantic Ocean in ocean reanalyses. *Geophysical Research Letters*, *42*, 2901–2909. https://doi.org/10.1002/2015GL063299

Häkkinen, S., Rhines, P. B., & Worthen, D. L. (2016). Warming of the Global Ocean: Spatial structure and water-mass trends. *Journal of Climate*, *29*(13), 4949–4963. https://doi.org/10.1175/jcli-d-15-0607.1

Hanawa, K., & Talley, L. D. (2001). Mode waters. In G. Siedler, J. Church, & J. Gould (Eds.), *Ocean circulation & climate: Observing and modelling the global ocean* (Vol. 77, pp. 373–386). New York: Academic Press. https://doi.org/10.1016/S0074-6142(01)80129-7

Hogg, N. G., & Johns, W. E. (1995). Western boundary currents. *Reviews of Geophysics*, *33*(S2), 1311–1334. https://doi.org/10.1029/95RG00491

Hogg, N. G., Pickart, R. S., Hendry, R. M., & Smethie, W. J. Jr. (1986). The northern recirculation gyre of the Gulf Stream. *Deep Sea Research Part A. Oceanographic Research Papers*, *33*(9), 1139–1165. https://doi.org/10.1016/0198-0149(86)90017-8

Huang, R. X. (2015). Heaving modes in the world oceans. *Climate Dynamics*, *45*(11-12), 3563–3591. https://doi.org/10.1007/s00382-015-2557-6

Iselin, C. (1936). A study of the circulation of the western North Atlantic. *Papers in Physical Oceanography and Meteorology*, *4*, 699–701.

Iselin, C., & Fuglister, F. C. (1948). Some recent developments in the study of the Gulf Stream. *Journal of Marine Research*, *7*, 317–329.

Joyce, T. M. (2012). New perspectives on eighteen-degree water formation in the North Atlantic. *Journal of Oceanography*, *68*(1), 45–52. https://doi.org/10.1007/s10872-011-0029-0

Joyce, T. M., & Zhang, R. (2010). On the path of the Gulf Stream and the Atlantic Meridional Overturning Circulation. *Journal of Climate*, *23*(11), 3146–3154. https://doi.org/10.1175/2010JCLI3310.1

Kamenkovich, I., Cheng, W., Schmid, C., & Harrison, D. E. (2011). Effects of eddies on an ocean observing system with profiling floats: Idealized simulations of the Argo array. *Journal of Geophysical Research*, *116*, C06003. https://doi.org/10.1029/2010JC006910

Kang, D., Curchitser, E. N., & Rosati, A. (2016). Seasonal variability of the Gulf Stream kinetic energy. *Journal of Physical Oceanography*, *46*(4), 1189–1207. https://doi.org/10.1175/JPO-D-15-0235.1

Kantha, L. H., & Clayson, C. A. (2000). *Numerical Models of Oceans and Oceanic Processes* (Vol. 66). San Diego: Academic Press. https://doi.org/10.1016/S0074-6142(00)80004-2

Kelly, K. A., & Dong, S. (2004). The relationship of western boundary current heat transport and storage to midlatitude ocean-atmosphere interaction. In C. Wang, S.-P. Xie, & J. A. Carton (Eds.), *Earth's climate: The ocean-atmosphere interaction* (pp. 347–364). Washington, DC: American Geophysical Union.

Kelly, K. A., & Dong, S. (2013). The relationship of western boundary current heat transport and storage to midlatitude ocean-atmosphere interaction. In *Earth's Climate* (pp. 347–363). Washington, DC: American Geophysical Union.

Kelly, K. A., Drushka, K., Thompson, L., Le Bars, D., & McDonagh, E. L. (2016). Impact of slowdown of Atlantic overturning circulation on heat and freshwater transports. *Geophysical Research Letters*, *43*, 7625–7631. https://doi.org/10.1002/2016GL069789

Kelly, K. A., Small, R. J., Samelson, R. M., Qiu, B., Joyce, T. M., Kwon, Y.-O., & Cronin, M. F. (2010). Western boundary currents and frontal air–sea interaction: Gulf Stream and Kuroshio Extension. *Journal of Climate*, *23*(21), 5644–5667. https://doi.org/10.1175/2010JCLI3346.1

Klymak, J. M., Shearman, R. K., Gula, J., Lee, C. M., D'Asaro, E. A., Thomas, L. N., et al. (2016). Submesoscale streamers exchange water on the north wall of the Gulf Stream. *Geophysical Research Letters*, *43*, 1226–1233. https://doi.org/10.1002/2015GL067152

Koszalka, I. M., & LaCasce, J. H. (2010). Lagrangian analysis by clustering. *Ocean Dynamics*, *60*(4), 957–972. https://doi.org/10.1007/s10236-010-0306-2

Kwon, Y.-O., & Riser, S. C. (2004). North Atlantic subtropical mode water: A history of ocean-atmosphere interaction 1961–2000. *Geophysical Research Letters*, *31*, L19307. https://doi.org/10.1029/2004GL021116

LaCasce, J. H. (2008). Statistics from Lagrangian observations. *Progress in Oceanography*, *77*(1), 1–29. https://doi.org/10.1016/j.pocean.2008.02.002

Levitus, S. (1982). *Climatological atlas of the world ocean*, NOAA Professional Paper 13, (U. S. G. P. Office ed.). Princeton, NJ: U.S. Gov. Printing Office.

Levitus, S., Antonov, J. I., Boyer, T. P., Baranova, O. K., Garcia, H. E., Locarnini, R. A., et al. (2012). World ocean heat content and thermosteric sea level change (0–2000 m), 1955–2010. *Geophysical Research Letters*, *39*, L10603. https://doi.org/10.11029/12012GL051106

Lévy, M., Klein, P., Tréguier, A. M., Iovino, D., Madec, G., Masson, S., & Takahashi, K. (2010). Modifications of gyre circulation by sub-mesoscale physics. *Ocean Modelling*, *34*(1), 1–15. https://doi.org/10.1016/j.ocemod.2010.04.001

Locarnini, R. A., Mishonov, A. V., Antonov, J. I., Boyer, T. P., Garcia, H. E., Baranova, O. K., et al. (2013). In S. Levitus (Ed.), *World ocean atlas 2013, volume 1: Temperature*, NOAA Atlas NESDIS (p. 40). Washington, DC: NOAA/NESDIS.

Lozier, M. S., Bacon, S., Bower, A. S., Cunningham, S. A., Jong, M. F. d., de Steur, L., et al. (2017). Overturning in the subpolar North Atlantic Program: A new international ocean observing system. *Bulletin of the American Meteorological Society*, *98*(4), 737–752. https://doi.org/10.1175/bams-d-16-0057.1

Lozier, M. S., Leadbetter, S., Williams, R. G., Roussenov, V., Reed, M. S. C., & Moore, N. J. (2008). The spatial pattern and mechanisms of heat-content change in the North Atlantic. *Science*, *319*(5864), 800–803. https://doi.org/10.1126/science.1146436

Madec, G. (2008). NEMO reference manual, ocean dynamic component: NEMO-OPA. *Preliminary version*. Note du Pole de modélisation, Institut Pierre-Simon Laplace (IPSL), France(27), 1288–1161.

Malone, R. C., Smith, R. D., Maltrud, M. E., & Hecht, M. W. (2003). Eddy-resolving ocean modeling. *Los Alamos Science*, *28*, 223–231.

Maze, G., Deshayes, J., Marshall, J., Tréguier, A.-M., Chronis, A., & Vollmer, L. (2013). Surface vertical PV fluxes and subtropical mode water formation in an eddy-resolving numerical simulation. *Deep Sea Research Part II: Topical Studies in Oceanography*, *91*, 128–138. https://doi.org/10.1016/j.dsr2.2013.02.026

McCartney, M. S., & Talley, L. D. (1982). The subpolar mode water of the North Atlantic Ocean. *Journal of Physical Oceanography*, *12*(11), 1169–1188. https://doi.org/10.1175/1520-0485(1982)012<1169:tsmwot>2.0.co;2

Monin, A. S. (1986). *An introduction into the theory of climate*. Dordrecht: D. Reidel Publishing Company. https://doi.org/10.1007/978-94-009-4506-7

Monin, A. S., & Yaglom, A. M. (1971). *Statistical fluid mechanics: Mechanics of turbulence. Volume 1* (Vol. 1). Cambridge, MA: MIT Press.

OBPG. (2015). MODIS aqua level 3 SST MID-IR monthly 9km nighttime v2014.0. *PO.DAAC, CA, USA. Dataset accessed [2018-06-26] at* https://doi.org/10.5067/MODAM-MO9N4

Oschlies, A. (2002). Improved representation of upper-ocean dynamics and mixed layer depths in a model of the North Atlantic on switching from eddy-permitting to eddy-resolving grid resolution. *Journal of Physical Oceanography*, *32*(8), 2277–2298. https://doi.org/10.1175/1520-0485(2002)032<2277:IROUOD>2.0.CO;2

Palmer, M. D., Roberts, C. D., Balmaseda, M., Chang, Y. S., Chepurin, G., Ferry, N., et al. (2015). Ocean heat content variability and change in an ensemble of ocean reanalyses. *Climate Dynamics*, *49*(3), 909–930. https://doi.org/10.1007/s00382-015-2801-0

Rhines, P. B. (1979). Geostrophic turbulence. *Annual review of fluid mechanics*, *11*(1), 401–441. https://doi.org/10.1146/annurev.fl.11.010179.002153

Rhines, P. B. (2001). Mesoscale eddies. In J. H. Steele (Ed.), *Encyclopedia of ocean sciences* (pp. 1717–1730). Oxford: Academic Press. https://doi.org/10.1006/rwos.2001.0143

Richardson, P. L. (2001). Florida Current, Gulf Stream, and Labrador Current. In J. H. Steele (Ed.), *Encyclopedia of ocean sciences* (2nd ed., pp. 554–563). Oxford: Academic Press. https://doi.org/10.1016/B978-012374473-9.00357-X

Rieck, J. K., Böning, C. W., Greatbatch, R. J., & Scheinert, M. (2015). Seasonal variability of eddy kinetic energy in a global high-resolution ocean model. *Geophysical Research Letters*, *42*, 9379–9386. https://doi.org/10.1002/2015GL066152

Roemmich, D., & Argo-Steering-Team (2009). Argo: The challenge of continuing 10 years of progress. *Oceanography*, *22*(3), 27–35.

Roemmich, D., Boebel, O., Freeland, H., King, B., LeTraon, P., Molinari, R., et al. (1998). On the design and implementation of Argo: An initial plan for a global array of profiling floats. Melbourne, Australia.

Rossby, T. (1999). On gyre interactions. *Deep Sea Research Part II: Topical Studies in Oceanography*, *46*(1-2), 139–164. https://doi.org/10.1016/S0967-0645(98)00095-2

Schmitz, W. J. Jr., & McCartney, M. S. (1993). On the North Atlantic circulation. *Reviews of Geophysics*, *31*(1), 29–49. https://doi.org/10.1029/92RG02583

Seidov, D., Baranova, O. K., Boyer, T., Cross, S. L., Mishonov, A. V., & Parsons, A. R. (2016). *Northwest Atlantic regional ocean climatology*, *NOAA Atlas NESDIS* (Vol. 80, p. 56). Washington, DC: NOAA/NESDIS.

Seidov, D., Mishonov, A., Reagan, J., Baranova, O., Cross, S., & Parsons, R. (2018). Regional climatology of the Northwest Atlantic Ocean: High-resolution mapping of ocean structure and change. *Bulletin of the American Meteorological Society*, *99*(10), 2129–2138. https://doi.org/10.1175/bams-d-17-0205.1

Seidov, D., Mishonov, A., Reagan, J., & Parsons, R. (2017). Multidecadal variability and climate shift in the North Atlantic Ocean. *Geophysical Research Letters*, *44*, 4985–4993. https://doi.org/10.1002/2017GL073644

Smeed, D. A., McCarthy, G., Cunningham, S. A., Frajka-Williams, E., Rayner, D., Johns, W. E., et al. (2014). Observed decline of the Atlantic Meridional Overturning Circulation 2004 to 2012. *Ocean Science*, *10*(1), 29–38. https://doi.org/10.5194/os-10-29-2014

Smith, S. (2013). *Digital signal processing: A practical guide for engineers and scientists*. Oxford, UK: Elsevier Science.

Steven, R. J., Roemmich, D., Zilberman, N., Riser, S. C., Johnson, K. S., Johnson, G. C., & Piotrowicz, S. R. (2017). The Argo program: Present and future. *Oceanography*, *30*(2), 18–28. https://doi.org/10.5670/oceanog.2017.213

Stommel, H. (1958). *The Gulf Stream*. Berkeley, CA: University of California.

Taylor, A. H., & Stephens, J. A. (1998). The North Atlantic Oscillation and the latitude of the Gulf Stream. *Tellus A*, *50*(1), 134–142. https://doi.org/10.1034/j.1600-0870.1998.00010.x

Thomson, R. E., & Emery, W. J. (2014). *Data analysis methods in physical oceanography* (3rd ed.). Amsterdam, Netherlands: Elsevier.

Thoppil, P. G., Richman, J. G., & Hogan, P. J. (2011). Energetics of a global ocean circulation model compared to observations. *Geophysical Research Letters*, *38*, L15607. https://doi.org/10.1029/2011GL048347

Treguier, A. M., Lique, C., Deshayes, J., & Molines, J. M. (2017). The North Atlantic eddy heat transport and its relation with the vertical tilting of the Gulf Stream axis. *Journal of Physical Oceanography*, *47*(6), 1281–1289. https://doi.org/10.1175/jpo-d-16-0172.1

Treguier, A. M., Theetten, S., Chassignet, E. P., Penduff, T., Smith, R., Talley, L., et al. (2005). The North Atlantic subpolar gyre in four high-resolution models. *Journal of Physical Oceanography*, *35*(5), 757–774. https://doi.org/10.1175/jpo2720.1

Werdell, P. J., Franz, B. A., Bailey, S. W., Feldman, G. C., Boss, E., Brando, V. E., et al. (2013). Generalized ocean color inversion model for retrieving marine inherent optical properties. *Applied Optics*, *52*(10), 2019–2037. https://doi.org/10.1364/AO.52.002019

Williams, R. G., Roussenov, V., Lozier, M. S., & Smith, D. (2015). Mechanisms of heat content and thermocline change in the subtropical and subpolar North Atlantic. *Journal of Climate*, *28*(24), 9803–9815. https://doi.org/10.1175/JCLI-D-15-0097.1

Willis, J. K., Roemmich, D., & Cornuelle, B. (2004). Interannual variability in upper ocean heat content, temperature, and thermosteric expansion on global scales. *Journal of Geophysical Research*, *109*, C12036. https://doi.org/10.1029/2003JC002260

World Meteorological Organization (2011). *Guide to Climatological Practices* (Vol. WMO-No. 100). Geneva, Switzerland: WMO.

Worthington, L. V. (1976). *On the North Atlantic circulation*. Baltimore, MD: Johns Hopkins University Press.

Wunsch, C. (1978). The North Atlantic general circulation west of 50°W determined by inverse methods. *Reviews of Geophysics*, *16*(4), 583–620. https://doi.org/10.1029/RG016i004p00583

Yashayaev, I., Seidov, D., & Demirov, E. (2015). A new collective view of oceanography of the Arctic and North Atlantic basins. *Progress in Oceanography*, *132*, 1–21. https://doi.org/10.1016/j.pocean.2014.12.012

Zhai, X., & Greatbatch, R. J. (2006). Inferring the eddy-induced diffusivity for heat in the surface mixed layer using satellite data. *Geophysical Research Letters*, *33*, L24607. https://doi.org/10.1029/2006GL027875

Zweng, M. M., Reagan, J. R., Antonov, J. I., Locarnini, R. A., Mishonov, A. V., Boyer, T. P., et al. (2013). In S. Levitus (Ed.), *World ocean atlas 2013, volume 2: Salinity*, *NOAA Atlas NESDIS* (p. 39). Washington, DC: NOAA/NESDIS.